Published in final edited form as:
Nano Lett. 2013 April 10; 13(4): 1736–1742. doi:10.1021/nl4003238.

Evolution of light-induced vapor generation at a liquid-immersed metallic nanoparticle

Zheyu Fang[1,5], **Yu-Rong Zhen**[2], **Oara Neumann**[1,2], **Albert Polman**[3], **F. Javier García de Abajo**[4], **Peter Nordlander**[1,2], and **Naomi J. Halas**[1,2]

Zheyu Fang: zhyfang@rice.edu; Peter Nordlander: nordland@rice.edu; Naomi J. Halas: halas@rice.edu

[1]Department of Electrical and Computer Engineering, Rice University, 6100 Main Street, Houston, Texas 77005, USA [2]Department of Physics and Astronomy, and Laboratory for Nanophotonics, Rice University, 6100 Main Street, Houston, Texas 77005, USA [3]Center for Nanophotonics, FOM Institute AMOLF, Science Park 104, 1098 XG Amsterdam, The Netherlands [4]IQFR - CSIC, Serrano 119, 28006 Madrid, Spain [5]School of Physics, State Key Lab for Mesoscopic Physics, Peking University, Beijing 100871, China

Abstract

When an Au nanoparticle in a liquid medium is illuminated with resonant light of sufficient intensity, a nanometer scale envelope of vapor -a “nanobubble”- surrounding the particle, is formed. This is the nanoscale onset of the well-known process of liquid boiling, occurring at a single nanoparticle nucleation site, resulting from the photothermal response of the nanoparticle. Here we examine bubble formation at an individual metallic nanoparticle in detail. Incipient nanobubble formation is observed by monitoring the plasmon resonance shift of an individual, illuminated Au nanoparticle, when its local environment changes from liquid to vapor. The temperature on the nanoparticle surface is monitored during this process, where a dramatic temperature jump is observed as the nanoscale vapor layer thermally decouples the nanoparticle from the surrounding liquid. By increasing the intensity of the incident light or decreasing the interparticle separation, we observe the formation of micron sized bubbles resulting from the coalescence of nanoparticle-“bound” vapor envelopes. These studies provide the first direct and quantitative analysis of the evolution of light-induced steam generation by nanoparticles from the nanoscale to the macroscale, a process that is of fundamental interest for a growing number of applications.

Keywords

Plasmonic heating; Au Nanoparticle; LSPR; Nanobubble; Microbubble

Recently it was demonstrated that metallic nanoparticles, suspended in liquids and illuminated by focused sunlight, can produce steam with remarkably high efficiency.[1] More than 80% of the power absorbed by the nanoparticles resulted in vaporization, while less than 20% of the absorbed power went into heating the liquid.[1] This result, occurring at a very low light intensity threshold (~10^6 W/m^2), has stimulated significant interest in the fundamental aspects of this process as well as its possible technological applications.[2] To develop and optimize this effect for applications, which range from medical and waste sterilization to water purification and distillation, it is crucial to develop a fundamental

Correspondence to: Zheyu Fang, zhyfang@rice.edu; Peter Nordlander, nordland@rice.edu; Naomi J. Halas, halas@rice.edu.

microscopic understanding of the vaporization process. Although no microscopic theory was initially proposed to explain the measured efficiencies, the authors noted that the results were consistent with a very simple model where a vapor envelope nucleates around each individual illuminated nanoparticle. The nanoparticle/vapor bubble complex expands under further illumination, eventually achieving buoyancy, moving toward the liquid/air interface and releasing the vapor, after which the nanoparticle reverts back into the solution and, as long as it is illuminated, repeats the process. Clearly an essential step in this process is the initial formation of a vapor layer around the illuminated nanoparticle.

Noble metal nanoparticles, when illuminated at a wavelength corresponding to their plasmon resonance, can serve as highly efficient localized heat sources at the nanometer length scale.[3-18] This is a unique and well established property that has enabled numerous applications across a range of fields including energy,[19-21] chemical catalysis,[4,8] protein imaging,[10,12] and biomedicine.[14,17] Several studies have also investigated bubble and vapor formation in ensembles of metallic nanoparticles under CW and pulsed laser excitation.[3-5,13,16,22-23] Despite these studies, the precise properties of the liquid-vapor phase transition at the nanoparticle surface, such as temperature, internal pressure, and size of the vapor envelope --the “nanobubble”-- formed upon resonant laser excitation, have not been investigated. Quantifying these properties at the single nanoparticle level is crucial for understanding the vapor generation process.

In this article, we investigate plasmon-induced vapor generation from an individual nanoparticle deposited on a substrate. We combine dark-field scattering measurements of localized surface plasmon resonance (LSPR) shifts with surface-enhanced Raman scattering (SERS)-based temperature measurements on individual, illuminated Au nanoparticles. These nano-optic probes were performed during controlled resonant laser excitation at incident intensities both below and above the threshold required to induce local vapor formation. This combination of local optical measurements at an individual nanoparticle allows us to determine several key microscopic parameters of this system, such as the nanobubble radius around the nanoparticle surface, the internal nanobubble pressure, the nanoparticle surface temperature, and their dependence on incident light intensity. For dense nanoparticle coverages and with further increases in incident light intensity, we observe the formation of micron sized bubbles due to the coalescence of nanobubbles centered on adjacent nanoparticles. We quantify the energetics of macroscopic bubble formation based on the incident laser power and the areal density of nanoparticle nucleation sites. This series of experiments provides a detailed picture of the light-induced steam formation process by resonant excitation of metallic nanoparticles which will be useful for the development and optimization of applications of this unique phenomenon.

Gold nanoparticles were chemically synthesized, then immobilized with an ultrathin layer of *poly*(4-vinyl pyridine)(PVP) onto a transparent dielectric substrate at the bottom of a microchamber (Fig1a). These nanoparticles were dispersed onto the substrate surface at a very dilute areal coverage, nominally 1 nanoparticle/100 μm^2 (Figure 1B shows a SEM image of a sample of deposited nanoparticles at significantly higher areal density, for visualization purposes; more details in the Methods section). The microchamber was designed to be optically probed by dark field microscopy (for LSPR spectroscopy) during simultaneous illumination by a CW “heating” laser beam. The CW resonant heating laser also served as the Raman pump laser for SERS studies of the heating of the nanoparticle surface. The microchamber could be evacuated for studies in ambient air, or filled with DI water.

Dark-field optical microspectroscopy[24-25] was used to detect changes in the individual nanoparticle LSPR scattering spectrum upon resonant laser illumination (Fig. 1c). The

measured LSPR spectrum in air was found to peak at 563 nm. When the microchamber was filled with DI water with a temperature of 20 °C, the LSPR was observed to redshift to 598 nm. The redshift of 35 nm is in good agreement with the redshift obtained from a Mie calculation for the same particle embedded in air compared with that in water at 20 °C (ε=1.778). During laser illumination while the nanoparticle was surrounded by water, however, the LSPR was observed to blueshift to 581 nm. The observed shift implies a decreased refractive index of the medium directly surrounding the nanoparticle, which we interpret as resulting from a water vapor envelope surrounding the nanoparticle. The incident light intensity threshold for the blueshift of the LSPR is approximately 2.5×10^{10} W/m^2, which is much larger than the light intensities used in the nanoparticle-enabled solar steam generation experiment. A likely reason for this difference is that the presence of the substrate forces a nonspherical shape for the nascent vapor bubble. The increased curvature of the vapor bubble near the nanoparticle/substrate interface should result in substantially increased surface tension, making bubble formation in this geometry far more difficult than for an isolated nanoparticle suspended in solution. Other effects that could be present for nanoparticles suspended in solution, such as multiple scattering and collective field enhancement effects,[26] may also be present to lower the energy threshold for an isotropic geometry relative to these substrate-bound, single nanoparticle experiments.

When illuminated by a CW laser, an Au nanoparticle is heated due to nonradiative plasmon decay. For low incident laser power, heat from the nanoparticle is transferred into the surrounding solution, resulting in a steady-state thermal gradient.[6] At higher incident powers (25 mW and above), a thin layer of surrounding water vaporizes and forms a nanobubble which provides a thermal barrier, reducing subsequent heat transfer into the surrounding solution. The size of the nanobubble is determined from a simple energy balance: the bubble expands until the power dissipated into the liquid becomes equal to the power absorbed by the nanoparticle from the incident laser light. The observed blueshift of the LSPR is far too large to be consistent with merely heating the surrounding liquid: for a gold nanoparticle of an equivalent size immersed in 100 °C water ambient, only a 3 nm blueshift would be observed (Fig. S1, Supplementary Information).

The rate of plasmon-induced heat generation in a nanoparticle is proportional to its optical absorption cross section multiplied by the incident optical intensity.[3-4] Since the absorption efficiency (absorption cross-section divided by the nanoparticle cross-section πR_{NP}^2) varies with nanoparticle size, the dependence of the blueshift on nanoparticle size was also investigated (Fig. 1d). A maximum blueshift of 18 nm was detected for Au nanoparticles of 100 nm, decreasing quite strongly for both smaller and larger nanoparticles. This trend clearly shows an optimal nanoparticle size for steam generation at 532 nm (See Fig. S2, Supplementary Information). For each illuminated particle, the light-induced heating power is a product of the incident light intensity by the absorption cross-section. For the optimal nanoparticle size of nominally 100 nm diameter, the laser induced heat generation in each particle is ~5×10^{-4} W. The reason for the reduction in blueshift for large nanoparticles is phase retardation with increasing size. The error bars reflect variations in the resonance blueshift measured for different particles with the same nominal size, which we attribute to the size and shape variation of chemically synthesized Au nanoparticles in each size range. This variation suggests a sensitivity of the steam nucleation threshold to details of nanoparticle morphology.

To directly measure the temperature at the nanoparticle surface during the bubble formation, we performed SERS on individual 100 nm diameter Au nanoparticles. The nanoparticles were functionalized with a monolayer of *para*-mercaptoaniline (pMA, 0.3 nm thick), shown previously to yield a robust SERS signal from individual nanoparticles under resonant laser pumping.[11] The SERS measurements were performed in the water-filled microchamber.

Optical vibrational pumping was observed, showing an evolution of the Raman response of the system as a function of incident laser power (Fig. 2) (the Stokes and anti-Stokes Raman spectra are shown in Figure S3). While several spectral peaks were observed in the Stokes spectrum, our analysis focused on the 390 cm^{-1} mode, which corresponds to the Au-S stretching mode associated directly with the chemical bond between the adsorbate molecules and the Au nanoparticle surface. A quadratic dependence of the anti-Stokes intensity on incident power is observed, as expected in the optical pumping regime (Fig. 2b).[27] A temperature was extracted from the ratio of the Stokes and anti-Stokes intensities for this vibrational mode using [11,15,18]

$$\frac{I_{AS}}{I_S} = A\left(\frac{E_0+E_{ph}}{E_0-E_{ph}}\right)^4 \exp\left(-\frac{E_{ph}}{k_B T}\right), \quad (1)$$

where I_{AS} and I_S are the anti-Stokes and Stokes Raman intensities for the mode, E_0 and E_{ph} are the photon and phonon energies, respectively, and A is a correction factor that accounts for the ratio of cross-sections for Stokes and anti-Stokes Raman scattering.

At low incident laser power (1 mW), the temperature obtained, assuming $A = 1$, was 289 K, corresponding within experimental error to the ambient temperature of the water prior to laser illumination (290 K). We therefore assumed that the cross-sections for Stokes and anti-Stokes scattering are similar, and set $A = 1$ for our subsequent analysis, which is reasonable since both Stokes and anti-Stokes cross sections are described by the same matrix element. Stokes and anti-Stokes spectra were obtained from the nanoparticle as incident laser power was increased, and the integrated areas of the 390 cm^{-1} mode peaks were converted to effective temperatures using Eqn. 1 (Fig. 2b). The temperature at the nanoparticle surface obtained in this manner was observed to increase smoothly and reversibly from 289 K to 379 K (±20 K) with increasing laser power. This reversibility implies that within this temperature range, the temperature of nanoparticle surface responds directly to the incident power, without any delay effects or hysteresis that would indicate a phase transition such as the formation of a vapor envelope around the nanoparticle, or a change in nanoparticle morphology or surface chemistry.

When the incident laser power was increased to 25 mW, corresponding to the threshold for nanobubble formation inferred from the LSPR shift, the Raman spectra exhibited large changes in intensity. Both the Stokes and Anti-Stokes intensities for the 390 cm^{-1} vibrational mode exhibit a dramatic jump after 60 seconds of illumination at this power level (Fig. 2c). From the Stokes and anti-Stokes data and Eqn. 1, we see that the observed spectral changes correspond to a rapid temperature increase from 400 K to 465 K (±3K) (in this regime of higher pump power levels, the error bars are within the symbols used to plot the data). This rapid temperature increase is consistent with the formation of a thermally insulating thin vapor layer around the nanoparticle. Once this initial layer is formed, the temperature of the nanoparticle and its surrounding vapor will increase until a new steady state determined by an energy balance between the incident power and the heat flow across the vapor/water interface of the vapor envelope, is reached. The final steady-state temperature of 465 K, deduced from the Raman spectra, corresponds to the nanoparticle temperature, since the pMA is bound to the Au surface. Because this temperature is measured independently from the LSPR experiment and is significantly lower than the temperature onset of 647K for spinodal decomposition of water, we do not believe that the measured LSPR shift is due to a local phase change of the water. The LSPR probing depth around a nanosphere of 100 nm only reaches a few tens of nanometers beyond the nanoparticle surface. Thus the measured LSPR shift cannot be explained by a large spinodal phase bubble with a weakly reduced refractive index, but instead requires a substantial reduction of the refractive index in the

immediate vicinity of the nanoparticle surface. Both these observations support our conclusion that a vapor layer surrounds the nanoparticles.

A schematic of the system is shown in Fig. 3a (for simplicity, the substrate is neglected). When the surface plasmon of the nanoparticle is excited by a laser, a part of the incident energy dissipates elastically into scattered photons, while the remainder results in heat. The calculated heat source density, that is, the generated heating power per unit volume for a 100 nm diameter Au nanoparticle, immersed in water and illuminated by a linearly polarized plane wave with the incident E field along the *y* axis, is shown in Fig. 3b. The "hottest" regions are at the "north" and "south" poles where the wavevector "enters" and "leaves" the sphere. This is quite distinct from the regions of the nanoparticle surface with the largest plasmon-induced field enhancements, which occur on the sides of the sphere aligned with the incident E field (Fig. 3c). The origin of this discrepancy is two-fold. First, the surface current driven by the tangential electric field is largest at the north and south poles of the particle due to the dipolar-like electric field distribution. Second, the electric field is normal to the particle surface at its east and west sides, and is decreased by a factor of $1/\varepsilon_{Au}$ inside the metal because of the requirement of electric displacement continuity at the particle surface. Although the heat source density is not spherically uniform, the thermalization and heat diffusion in the gold particle are extremely fast relative to the heat diffusion through the steam and water, and thus we expect the metal nanoparticle to be effectively at a uniform temperature.

Since the observed LSPR blueshift of the nanoparticle is smaller than that for an infinite embedding medium of water vapor, we can use this information to estimate the bubble radius R_B. Within an electrostatic dipole model,[28-29] the redshift of the dipolar surface plasmon resonance is proportional to the relative permittivity change:

$$\frac{\Delta\lambda_B}{\Delta\lambda_w}=\frac{\Delta\varepsilon_B^{(eff)}}{\Delta\varepsilon_w}\equiv\frac{\varepsilon_B^{(eff)}-\varepsilon_{air}}{\varepsilon_w-\varepsilon_{air}}, \quad (2)$$

where $\Delta\lambda_B$ is the experimental redshift of the plasmon resonance for a nanoparticle in a finite nanobubble, $\Delta\lambda_w$ is the redshift of the plasmon resonance in water relative to its value for steam, $\Delta\varepsilon_B^{(eff)}$ is the permittivity increase for a finite nanobubble relative to steam, and $\Delta\varepsilon_w$ is the permittivity increase for water relative to steam. The superscript "*eff*" denotes the effective permittivity change experienced by the nanosphere. Assuming the geometry depicted in Fig. 3a, the values of ε=1.0 for steam (verified below) and ε=1.77 for water at room temperature, we performed Mie calculations[30-31] to obtain theoretical scattering spectra for different values of the bubble radius. From comparison of the measured value of $\Delta\lambda_B/\Delta\lambda_w$=0.51 (Fig. 1c) to the calculated spectra, we deduce that the thickness of the vapor shell around a single Au nanoparticle is nominally 6.5 nm (R_B = 56.5 nm) (See Supplementary Information, Figure S4). The LSPR measurement provides strong and consistent evidence that a nanosize bubble is generated. The spectral shift, calculated from Mie theory, agrees with the experimental scattering spectra using the concentric steam-water shell model where R_B = 56.5 nm (Fig. 3d).

The conventional model for plasmon induced bubble formation has recently been challenged.[1] In the conventional model, the temperature increase at the particle surface is calculated as $\Delta T = \sigma * I/(4\pi * k * R_{NP})$, where σ is the particle absorption cross section, I is the incident intensity, and k is the thermal conductivity of embedding material.[26] By considering the presence of the glass substrate and using the thermal conductivity (~1.6$Wm^{-1}K^{-1}$) of glass around 500 K, this model leads to an estimated particle temperature of at least 774 K. If the thermal conductivity of water is used, an even higher temperature results, in direct conflict with the observed 465 K from our Raman experiment. We notice that the calculation

of temperature in this model is based on energy dissipation by a total conductive heat transfer process. However, it is well known that other heat transfer processes such as convection can also increase the effective thermal conductivity. Therefore we speculate that the discrepancy between our measured temperature and the result from the conventional model is due to the neglect of fluid convection. The conventional model assumes a stationary fluid and only conductive heat transfer.

Once the bubble is formed, there is an alternative approach for determination of the temperature by using the equation of state for saturated steam: Clausius-Clapeyron Relation (CCR). The CCR approach does not depend on the balance between the heating power and the dissipated power, and thus is independent of the complexity of combinations of various heat transfer channels (through water, glass, convection, etc). Instead, the CCR approach depends on only one unknown parameter: the bubble size which has been directly determined from our LSPR experiments. With the nanobubble radius determined, the temperature and pressure of the confined steam within the nanobubble can be estimated as follows. We assume that the system reaches steady state after bubble formation, as suggested in Fig. 2c and 2d. At equilibrium, the Laplace pressure due to the surface tension at the water-steam interface is balanced by the vapor pressure of the steam, which is a function of temperature given by the Clausius-Clapeyron Relation. Hence, we have $C \exp(h / k_B T_s) = p_0 + 2\gamma(T_s) / R_B$, where C is a constant, h is the enthalpy of water evaporation, T_s is the temperature of saturated steam inside the bubble, p_0 is the atmospheric pressure (1 atm), and γ is the surface tension coefficient (See Supplementary Information, Text S1). The calculated steam temperature T_s within the nanobubble is 464K, with a corresponding internal pressure of 1.49 MPa (14.7 atm). This large pressure is essentially a consequence of the large surface tension for a bubble of nanoscale dimensions. At this pressure and temperature, the dielectric permittivity of steam is close to 1.0, consistent with the assumption made in the Mie calculation of steam layer thickness.

The temperature of the nanoparticle can also be calculated by applying Fourier's law at the gold-vapor interface: $P_{abs} = G_{g,s} S_{NP} (T_{NP} - T_s)$, where P_{abs} is the power absorbed by the Au NP, $G_{g,s}$ is the effective interfacial thermal conductance, S_{NP} is the surface area of the nanoparticle and T_{NP} is the NP surface temperature. The temperature difference ($T_{NP} - T_s$) is estimated to be approximately 63K from a gold-steam interfacial thermal conductance of 298 MW/(m^{2}K) (See Supplementary Information, Text S1, for a detailed calculation), resulting in an estimated nanoparticle surface temperature of T_{NP} =527K. The estimated average temperature of the molecular layer at the gold-vapor interface then was found to be 496K, which is a bit higher but close to the Raman experimental value of 465 K obtained from our SERS measurements. This difference is most likely due to our neglect of the dielectric substrate, which serves as a heat sink as compared with water. It is worth noting that the analysis of the interfacial thermal conductance (Supplementary Information) is an essential step for final determination of the surface temperature of the gold nanosphere from the steam temperature calculated in our approach. In fact, there are two competing cooling rates: one controlled by the effusivity of the fluid and one determined by the interface effect as discussed by Ge et. al.[32] Such a competition is very important for transient temporal evolution of temperature, i. e. in a pulsed-laser study.[32] However, it is not relevant here because we use continuous-wave laser illumination and the system is expected to be in steady state after the bubble is formed. Once a steady state is formed, the heating power is balanced by the power dissipated through fluid effusivity and heat transfer across the interfaces. There is no need to consider the competition between these two mechanisms since in a steady state we are not interested in the cooling rates but the temperature difference across the interface.

To study the transition from discrete nanobubbles localized on their individual, parent nanoparticles to optically observable, micron sized bubbles, the incident light intensity needs to be increased above the 25mW threshold and/or the nanoparticle density on the substrate needs to be increased. A time series of images under these new conditions, resulting in the formation of a microbubble, is shown in Figure 4a. After illumination (t=10.6 sec), a 1 μm bright spot (bubble) appears in the image, and after t=13.0 sec it has expanded to a microbubble of 10 μm diameter, with a volume encompassing approximately 5000 nanoparticles. We believe that the origin of the observed microbubbles is the coalescence of individual nanobubbles centered on adjacent nanoparticles, as illustrated in Fig. 4b. With increasing light intensity, the radii of the nanobubbles increase. If the interparticle spacing is sufficiently small, nanobubbles centered on adjacent nanoparticles will touch and coalesce, resulting in the formation of a larger microbubble encompassing several nanoparticles. Similar attraction-and-coalescence has also been observed for microbubbles.

The final size of the microbubble is a function of both incident power and nanoparticle separation. This is shown in the contour plot in Figure 4c, where the color map represents final bubble size as a function of these two parameters (the incident laser spot size is 5 μm). This contour plot is a result of an extended series of experimental measurements for multiple interparticle distances and input laser powers (all actual data values can be found in the Supplementary Information, Table 1). Generally speaking, higher incident powers (≥ 400 mW) and shorter interparticle separations (≤ 0.4 μm) result in a larger bubble size. We observe a strong sensitivity to interparticle distance: for large interparticle separations, only small microbubbles can be observed, even at the highest laser powers. This reflects the fact that the total energy absorbed within the laser spot of 5 microns is due to the total number of nanoparticles within the beam spot, a number which grows as the inverse square of the interparticle separation. In an isotropic environment we would anticipate that, for a specific bubble radius (single-colour contours of Fig. 4c) the input power would scale with the inverse square of the interparticle distance. The data measured here deviates from that simple scaling, most likely due to the additional loss introduced by the nanoparticle substrate.

In conclusion, we have examined the phenomenon of light-induced vapor generation at a plasmonic nanoparticle surface, from the initial formation of a nanoscale vapor envelope around an individual nanoparticle to the evolution of micron-scale bubbles due to coalescence of the expanded vapor envelopes. Our single-particle studies of vapor generation enable a detailed characterization of the size, pressure and temperature of the nascent nanobubble formed at a nanoparticle surface. The combination of quantitative measurements at the single nanoparticle level and rigorous analysis provides us with the first detailed picture of the vapor generation process at its initial stages. Our approaches for characterizing vapor formation should prove to be useful in the study of other local energetic processes, such as catalysis and local chemical or material-growth reactions. The studies reported here ultimately pave the way for a better understanding of the vapor generation process, which has captured a tremendous amount of recent interest for its potential applications, such as waste and water remediation at remote locations.

Methods

Sample preparation

Au nanoparticles with differing diameters ranging from 30 to 200 nm (NanoXact, Ted Pella, Inc.) were randomly dispersed and immobilized on the microchamber bottom surface, which was functionalized with poly(4-vinyl pyridine)(PVP). For single nanoparticle detection, a transmission electron microscope (TEM) sample grid was used to fabricate fiduciary marks by e-beam evaporation. In order to prevent the influence from other Au nanoparticles, the

selected nanoparticle was the only one found within the 10 μm ×10 μm sampling area. The microchamber was fabricated using 3M tape with a diameter of 1 cm and thickness of 80 μm. The chamber was sealed by a thin glass cover slide. The temperature of the microchamber and of the injected water was kept constant at 285 K. A thermograph was used to monitor any temperature change during the experimental measurements.

Experimental setup and measurements

The sample was placed on a piezoelectric positioning stage (Nanonics Co.) held by a *xyz* coarse adjustment stage (Newport Co.). A long working distance (12 mm) objective lens (Mitutoyo NIR 100X) with a numerical aperture 0.5 was used to focus a 532 CW laser beam onto the Au NP at normal incidence. The focus diameter was measured by moving a razor edge with the piezoelectric positioning stage, assuming a Gaussian beam profile. A white light source (MI-150, Edmond Optics) was used to illuminate the sample at oblique incidence. The dark-field scattering signals passed through the same objective lens and were detected by a monochrometer (Acton SP2150, PI) with a CCD camera (PIXIS400, PI). For the Raman measurements, a monolayer of p-mercaptoaniline (pMA) (~0.3 nm) was bound to the Au nanoparticle surface, and SERS measurements were performed with a microchamber filled with pure water. The signal was recorded by a Raman spectrometer (Acton SpectraPro2300i, PI) along the same experimental optical path. Microbubble generation was imaged using a CCD camera.

Supplementary Material

Refer to Web version on PubMed Central for supplementary material.

Acknowledgments

We thank the following agencies for their support of this research: The Robert A. Welch Foundation (C-1220, NH) and (C-1222, PN), The Air Force Office of Scientific Research (FA9550-10-1-0469, NH), the DoD NSSEFF (N00244-09-1-0067, NH and PN), the NIH NCI (U01 CA151886-01, NH and PN), and the Bill and Melinda Gates Foundation (OPP1044571, NH). Work at AMOLF is part of the research program of FOM and is also supported by the European Research Council.

References

1. Neumann O, et al. Solar Vapor Generation Enabled by Nanoparticles. ACS Nano. 2012
2. Polman A. Solar Steam Nanobubbles. ACS Nano. 2013
3. Govorov AO, Richardson HH. Generating heat with metal nanoparticles. Nano Today. 2007; 2:30–38.
4. Adleman JR, Boyd DA, Goodwin DG, Psaltis D. Heterogenous Catalysis Mediated by Plasmon Heating. Nano Lett. 2009; 9:4417–4423. [PubMed: 19908825]
5. Boyd DA, Greengard L, Brongersma M, El-Naggar MY, Goodwin DG. Plasmon-assisted chemical vapor deposition. Nano Lett. 2006; 6:2592–2597. [PubMed: 17090097]
6. Baffou G, Quidant R, de Abajo FJG. Nanoscale Control of Optical Heating in Complex Plasmonic Systems. ACS Nano. 2010; 4:709–716. [PubMed: 20055439]
7. Boyd DA, Adleman JR, Goodwin DG, Psaltis D. Chemical separations by bubble-assisted interphase mass-transfer. Anal Chem. 2008; 80:2452–2456. [PubMed: 18321130]
8. Christopher P, Xin HL, Linic S. Visible-light-enhanced catalytic oxidation reactions on plasmonic silver nanostructures. Nat Chem. 2011; 3:467–472. [PubMed: 21602862]
9. Huth F, Schnell M, Wittborn J, Ocelic N, Hillenbrand R. Infrared-spectroscopic nanoimaging with a thermal source. Nat Mater. 2011; 10:352–356. [PubMed: 21499314]
10. Ibrahimkutty S, et al. Ultrafast Structural Dynamics of the Photocleavage of Protein Hybrid Nanoparticles. ACS Nano. 2011; 5:3788–3794. [PubMed: 21504177]

11. Jackson JB, Halas NJ. Surface-enhanced Raman scattering on tunable plasmonic nanoparticle substrates. P Natl Acad Sci USA. 2004; 101:17930–17935.
12. Lee J, Govorov AO, Kotov NA. Nanoparticle assemblies with molecular springs: A nanoscale thermometer. Angew Chem Int Edit. 2005; 44:7439–7442.
13. Li C, et al. Nanostructured copper interfaces for enhanced boiling. Small. 2008; 4:1084–1088. [PubMed: 18570277]
14. Lim ZZJ, Li JEJ, Ng CT, Yung LYL, Bay BH. Gold nanoparticles in cancer therapy. Acta Pharmacol Sin. 2011; 32:983–990. [PubMed: 21743485]
15. Oron-Carl M, Krupke R. Raman spectroscopic evidence for hot-phonon generation in electrically biased carbon nanotubes. Phys Rev Lett. 2008; 100
16. Richardson HH, Carlson MT, Tandler PJ, Hernandez P, Govorov AO. Experimental and Theoretical Studies of Light-to-Heat Conversion and Collective Heating Effects in Metal Nanoparticle Solutions. Nano Lett. 2009; 9:1139–1146. [PubMed: 19193041]
17. von Maltzahn G, et al. Nanoparticles that communicate in vivo to amplify tumour targeting. Nat Mater. 2011; 10:545–552. [PubMed: 21685903]
18. Ward DR, Corley DA, Tour JM, Natelson D. Vibrational and electronic heating in nanoscale junctions. Nat Nanotechnol. 2011; 6:33–38. [PubMed: 21151112]
19. Atwater HA, Polman A. Plasmonics for improved photovoltaic devices. Nat Mater. 2010; 9:205–213. [PubMed: 20168344]
20. Erickson D, Sinton D, Psaltis D. Optofluidics for energy applications. Nature Photonics. 2011; 5:8.
21. Schuller JA, Taubner T, Brongersma ML. Optical antenna thermal emitters. Nature Photonics. 2009; 3:658–661.
22. Carlson MT, Green AJ, Richardson HH. Superheating Water by CW Excitation of Gold Nanodots. Nano Lett. 2012; 12:1534–1537. [PubMed: 22313363]
23. Lukianova-Hleb E, et al. Plasmonic Nanobubbles as Transient Vapor Nanobubbles Generated around Plasmonic Nanoparticles. ACS Nano. 2010; 4:2109–2123. [PubMed: 20307085]
24. Anderson LJE, et al. Quantitative Measurements of Individual Gold Nanoparticle Scattering Cross Sections. J Phys Chem C. 2010; 114:11127–11132.
25. Sonnichsen C, et al. Spectroscopy of single metallic nanoparticles using total internal reflection microscopy. Appl Phys Lett. 2000; 77:2949–2951.
26. Govorov AO, et al. Gold nanoparticle ensembles as heaters and actuators: melting and collective plasmon resonances. Nanoscale Res Lett. 2006; 1:84–90.
27. Galloway CM, Le Ru EC, Etchegoin PG. Single-molecule vibrational pumping in SERS. Phys Chem Chem Phys. 2009; 11:7372–7380. [PubMed: 19690708]
28. Jain PK, El-Sayed MA. Noble Metal Nanoparticle Pairs: Effect of Medium for Enhanced Nanosensing. Nano Lett. 2008; 8:4347–4352. [PubMed: 19367968]
29. Miller MM, Lazarides AA. Sensitivity of metal nanoparticle surface plasmon resonance to the dielectric environment. J Phys Chem B. 2005; 109:21556–21565. [PubMed: 16853799]
30. de Abajo FJG. Multiple scattering of radiation in clusters of dielectrics. Phys Rev B. 1999; 60:6086–6102.
31. Myroshnychenko V, et al. Modelling the optical response of gold nanoparticles. Chem Soc Rev. 2008; 37:1792–1805. [PubMed: 18762829]
32. Ge ZB, Cahill DG, Braun PV. AuPd metal nanoparticles as probes of nanoscale thermal transport in aqueous solution. J Phys Chem B. 2004; 108:18870–18875.

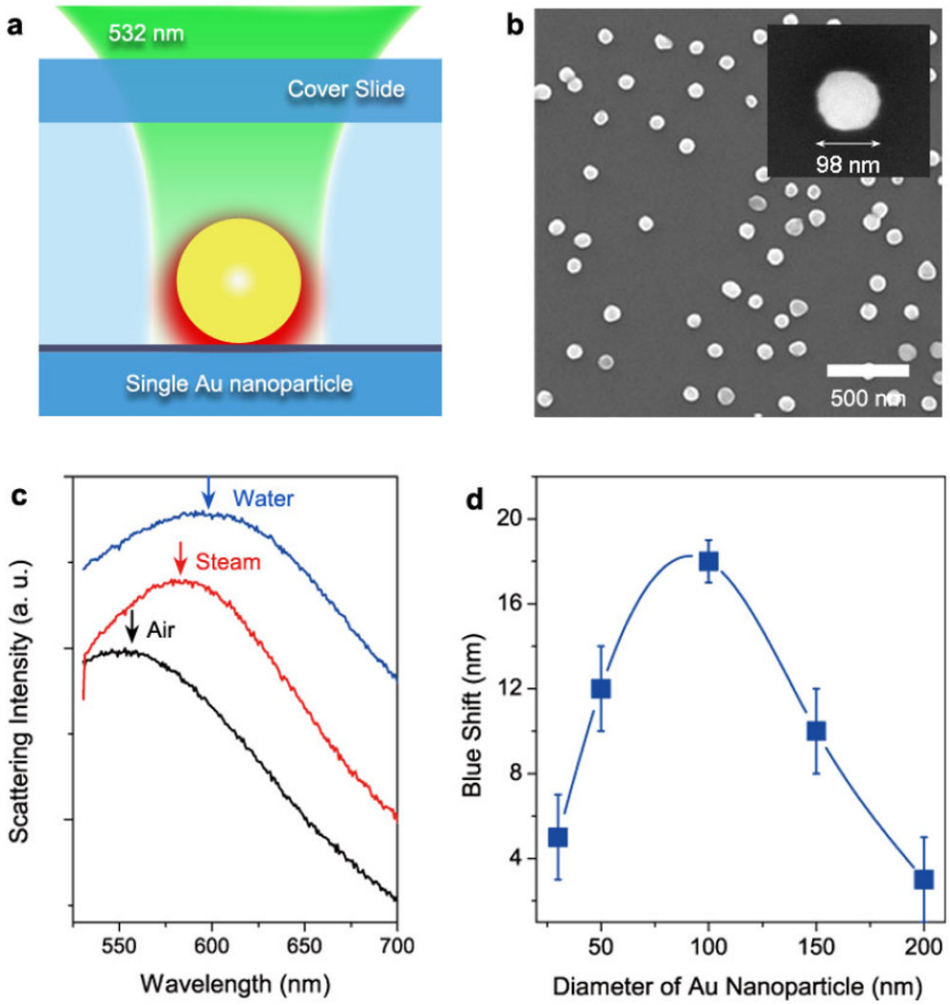

Figure 1. Light-induced generation of a nanobubble at a single nanoparticle surface

a. Schematic showing illumination and plasmonic heating of an individual Au nanoparticle on the transparent glass substrate floor of our fluidic microchamber. **b**. Scanning electron microscope (SEM) images of a sample with a dense coverage of Au nanoparticles randomly distributed on the glass substrate, and a typical nanoparticle (inset). **c**. Scattering intensities of a single 100-nm diameter nanoparticle in air (black), water (blue), and an envelope of water vapor produced by laser illumination (red). The blueshift corresponds to formation of a finite vapor envelope of nanometer scale thickness around the nanoparticle. Spectra are shifted vertically for clarity. The red curve corresponds to a vapor envelope thickness of 6.5 nm. **d**. Dependence of nanobubble-induced LSPR blueshift on Au nanoparticle diameter, with a maximum shift observed for a nanoparticle diameter of 100 nm. The error bars represent the nanoparticle-to-nanoparticle variation in the LSPR blueshift observed for a set of several (<10) nanoparticles. The incident laser power at 532 nm was 25 mW focused to a 1 μm diameter spot.

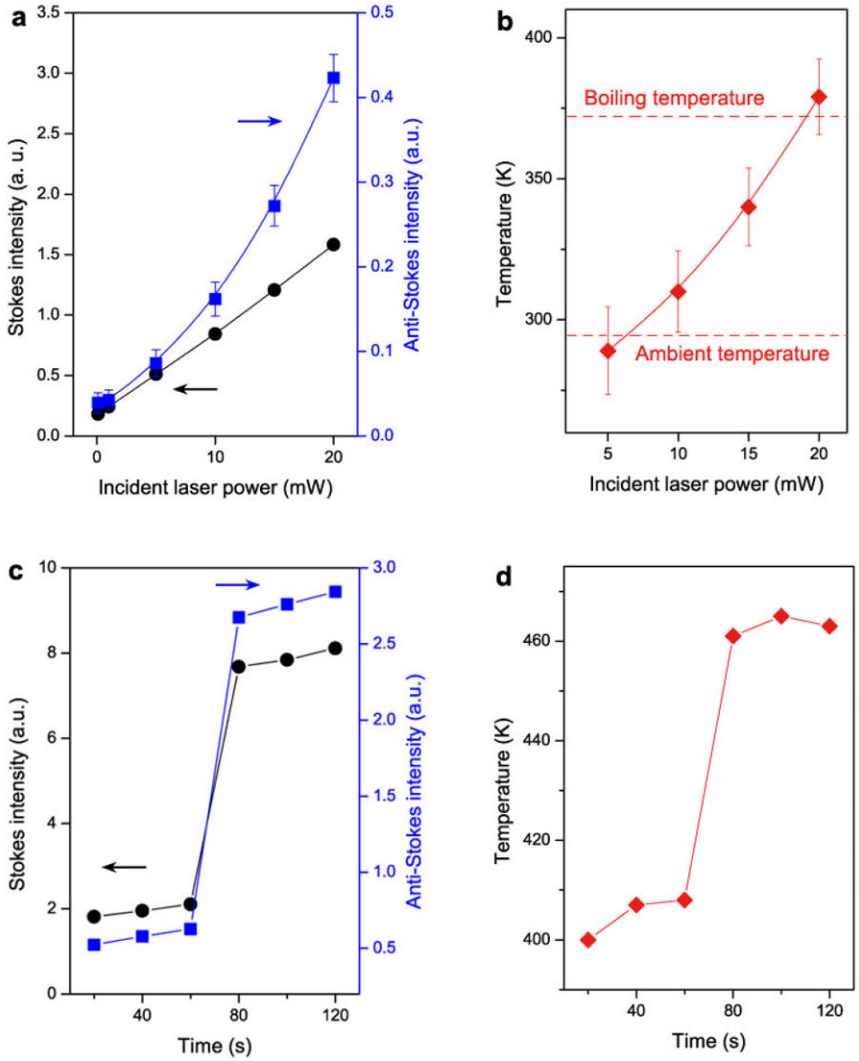

Figure 2. Temperature at the Au nanoparticle surface during the steam generation process

a. Power dependence of the Au-S Stokes (black dots) and anti-Stokes (blue squares) mode amplitudes at |390| cm^{-1} for a pMA-coated single Au NP (100 nm diameter) as a function of incident laser power. **b**. Temperature obtained from the mode amplitudes in **a** and Eqn. 1, as a function of incident pump laser power. Error bars in panels **a** and **b** indicate the uncertainty in the signal due to the low anti-Stokes signal levels in this range of incident laser intensities. **c**, Time dependence of Stokes (black dots) and anti-Stokes (blue squares) signals with 25 mW laser excitation. A large intensity jump occurs after 60 s of laser excitation. **d**, Temperature jump obtained from the mode amplitudes shown in **c** and Eqn. 1 occurring after 60 s of 25 mW laser excitation. The 532 nm light was focused on a 1 μm diameter spot.

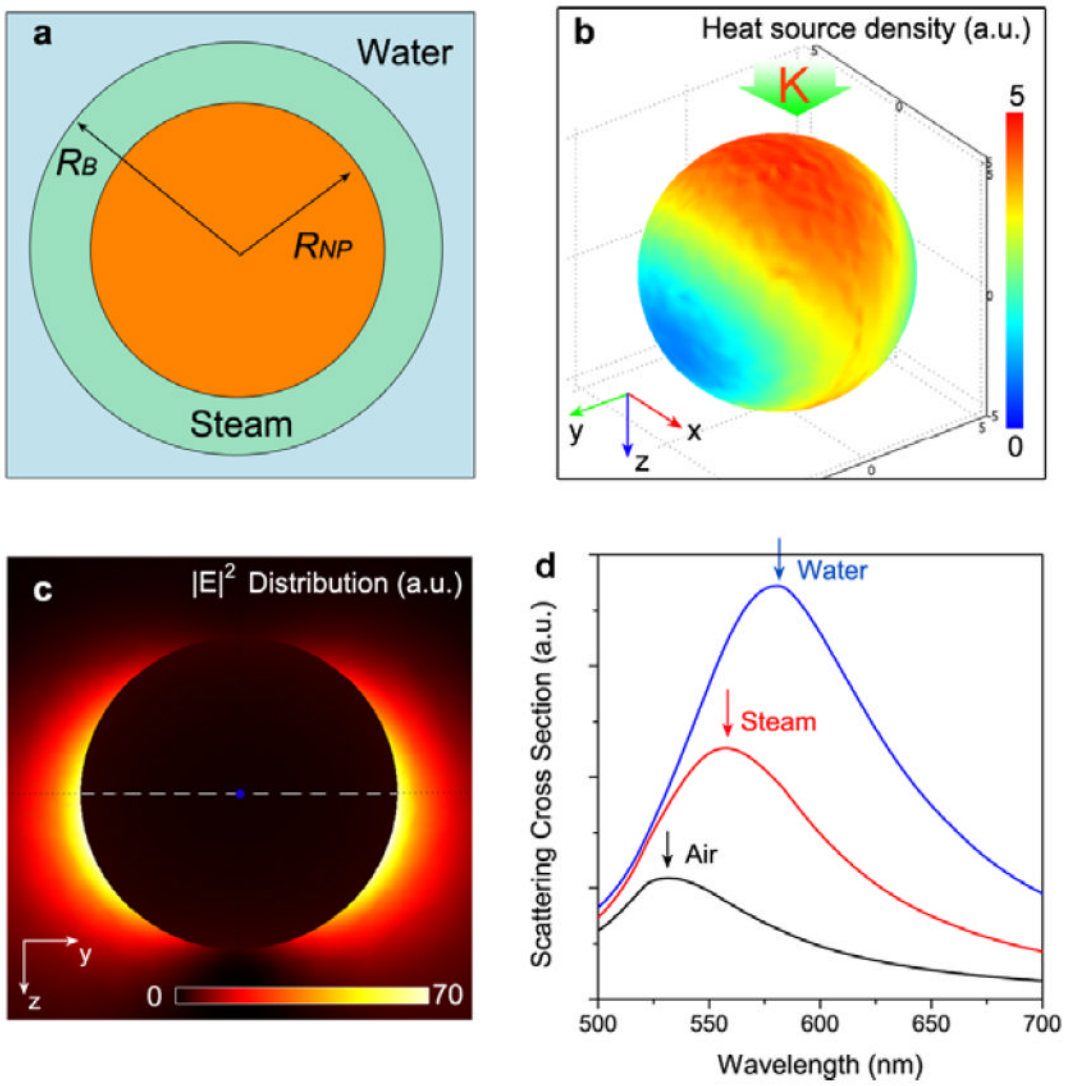

Figure 3. Nanobubble theoretical modeling

a. Schematic of nanobubble formation around a nanoparticle under 532 nm resonant laser illumination. The nanobubble is a dielectric spacer layer of outer radius R_B between the nanoparticle surface (with radius R_{NP}) and the surrounding water medium. **b**. Simulated heat-source density for an illuminated 100 nm diameter Au nanoparticle immersed in water. Light is incident along the *z* axis and linearly polarized along *y*. **c**. Near-field intensity enhancement for a 100 nm diameter Au nanoparticle in water, relative to incident field intensity, under the same incidence and polarization conditions as in b. **d**. Mie calculation of the scattering cross-sections for a 100-m diameter Au NP in air (black), surrounded by a steam bubble with outer radium R_B= 60 nm (red), and in water (blue). The simulation for the steam layer is in good agreement with the experimental observations in Fig. 1c.

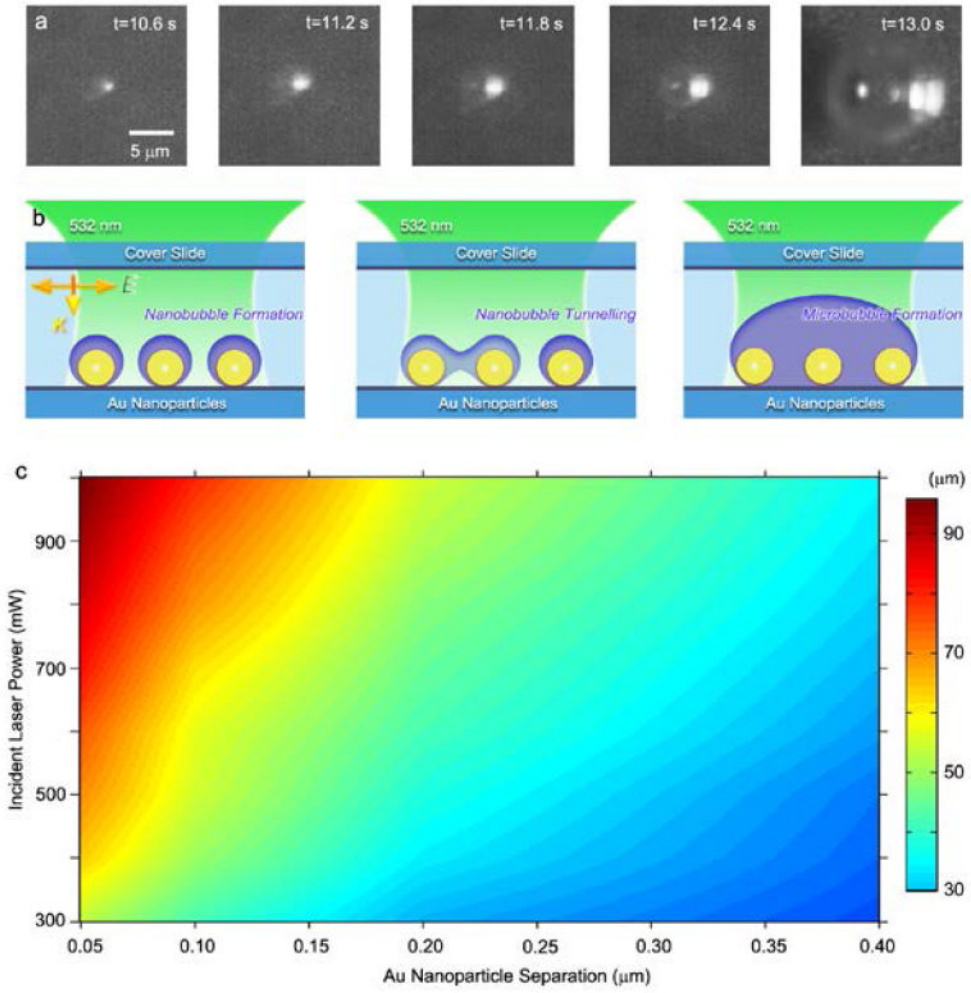

Figure 4. Coalescence of nanobubbles into micron-sized bubbles

a. Time series of microbubble generation. The nanoparticle areal density is 3×10^{8} cm^{-2} (average NP-NP separation ~0.5 μm). **b**. Schematics depicting microbubble formation due to the coalescence of neighboring nanobubbles produced on individual Au nanoparticles. **c**, Experimental diagram of the dependence of final bubble size and formation time on incident laser power and average nanoparticle separation, where the color indicates final bubble diameter (scale bar on right). The 532 nm light was focused on a 5 μm diameter spot.